

## Hot-electron influence on the x-ray emission spectra of Ar clusters heated by a high-intensity 60-fs laser pulse

J. Abdallah, Jr.

*Theoretical Division, T-4, Los Alamos National Laboratory, P.O. Box 1663, Los Alamos, New Mexico 87545*

A. Ya. Faenov, I. Yu. Skobelev, A. I. Magunov, and T. A. Pikuz  
*Multicharged Ions Spectra Data Center of VNIIFTRI, Mendeleev, 141570 Russia*

T. Auguste, P. D'Oliveira, S. Hulin, and P. Monot  
*Commissariat à l'Energie Atomique, Centre D'Etudes de Saclay, DSM/DRECAM, Service des Photons Atomes et Molécules, Bâtiment 522, 91191 Gif-sur-Yvette cédex, France*  
(Received 2 August 2000; published 7 February 2001)

The interaction of a high-intensity 60-fs laser pulse with argon clusters is investigated experimentally using methods of x-ray spectroscopy. It is shown that the plasma emission in the vicinity of He-like Ar XVII resonance line contains intense satellites caused by transitions in Li-like, Be-like, and other argon ions. It is shown that observed spectra could be explained by the presence of hot electrons in moderately ionized plasma. A simple physical model of plasma creation is proposed involving the incident picosecond prepulse followed by the main laser femtosecond pulse. Atomic kinetic calculations based on the proposed model give a good description of the experimental data.

DOI: 10.1103/PhysRevA.63.032706

PACS number(s): 36.40.Vz, 52.25.Os

### I. INTRODUCTION

Recently there have been many investigations of the interaction of radiation from ultrashort laser pulses with both solid and gas targets. These studies provided knowledge about fundamental properties of matter under critical conditions, as well as solutions for different applications, such as ignition of nuclear reactions, heavy particle acceleration, construction of the bright x-ray sources for medicine, biology, lithography, etc.; see, for example, Refs. [1–3].

There are very significant differences between the interaction physics observed in solid and gas targets, and the plasma conditions produced in these two media are correspondingly quite distinct. Solid targets irradiated by high-intensity subpicosecond laser pulses can produce near-solid density plasmas with electron temperatures of several hundreds of eV. In contrast, monatomic gas targets are inefficient absorbers of laser radiation, and relatively cold plasmas with temperatures well below 100 eV are produced mainly by multiphoton and field ionization processes. There are a number of targets that might prove suitable to fill gap between solids and gases. Atomic clusters are an important candidate because they can be produced in a broad range of sizes from a few atoms to well in excess of 1 000 000 atoms per cluster. Some aspects of cluster behavior in intense laser field are similar to those of solids or gases, but they also show several quite unique effects; see, for example, Refs. [1, 3–12].

In addition to the target state, the properties of the laser pulse are also important for determining the physics of interaction of ultrashort laser pulses with matter. For example, one very important property is the amount of prepulse that precedes the main pulse. Contrast is defined as the flux density of the prepulse divided by that of the main pulse. If the contrast of a subpicosecond pulse is relatively small, then the

intensity of the prepulse is significant, and the main laser pulse interacts with plasma that is already formed by the prepulse. In this case, even with solid targets, it is impossible to create plasmas with near solid density and the main laser pulse actually interacts with a “plasma target.” This type of target can also be produced when high-intensity subpicosecond laser pulses interact with large clusters.

Irradiation of all types of targets, including solids, gases, clusters, and plasma, by a subpicosecond laser produces a bright source of x-ray radiation, which is caused by collisions of plasma electrons with ions resulting in the population of excited atomic levels that consequently emit through spontaneous decay. The main radiative features of these plasmas are observed in the resulting emission spectra. Hence x-ray spectroscopy is used extensively for diagnostic studies of subpicosecond laser-produced plasmas, and most of the information on the properties of such plasmas was obtained using this experimental technique. Distinct differences in the observed spectra show the dominant role of processes that were of little importance for plasmas created by nanosecond laser pulses. The most significant differences were found in high-contrast subpicosecond laser pulse interactions with solid targets [13–17]. In this case, the effective formation of “so-called” hollow ion states occurs due to high plasma density, and the x-ray emission spectra differs drastically from analogous spectra observed in experiments with nanosecond lasers.

An additional characteristic of subpicosecond laser-produced plasmas is not only superhigh density but also the generation of fast ions and electrons. The presence of fast particles must also affect the emission spectra. For example, fast motion of ions must lead to deformation of spectral line profiles due to the Doppler effect [10,11,18], while fast electrons can change the ion population kinetics and consequently change the relative intensities of various spectral

lines; see, for example, Refs. [19–21]. Solid targets are not optimal for observing these effects because high-density plasma can mask the role of fast particles.

In the present paper, we study the effect of fast electrons on the x-ray emission spectra of a femtosecond laser-produced-plasma for a “plasma target” that was created by the interaction of picosecond laser prepulse with large argon clusters. A simple physical model for the plasma dynamics is proposed in conjunction with detailed quasistationary collisional-radiative kinetics calculations. The model is shown to correctly describe the x-ray spectrum that is observed. An estimate of the number of fast electrons and the plasma conditions are obtained by comparing the calculated and experimental spectra.

## II. EXPERIMENTAL SETUP

The experiments were performed on the UHI10 laser. It is a two-beam 10-Hz Ti:sapphire laser system with wavelength  $\lambda = 800$  nm. The main beam has a 10-TW peak power. The low-energy ultrashort pulse is produced by a modified commercial Ti:sapphire oscillator that is stretched up to 300 ps by an aberration-free Offner stretcher. After four amplification stages, the pulse energy is about 1.2 J (600 mJ after recompression). The pulse is then recompressed down to 60 fs in a vacuum chamber that is directly connected to the experimental chamber. A small amount of the energy is peaked up between the third and fourth amplifiers, and is then sent to a second compressor. This beam has a 4-mJ energy (after recompression), and the pulse is recompressed in air. The contrast is measured to be about  $10^{-5}$  at 1 ps on the main beam with a high dynamic cross-correlator. The post-pulse and prepulse amplitudes are less than  $10^{-5}$ . The 80-mm-diameter laser beam is focused with an  $f/6.25$  off-axis parabolic mirror. The  $1/e^2$  focal spot radius is  $w_0 = 25 \mu\text{m}$  ( $M^2 \sim 4$ ). The corresponding Rayleigh length and vacuum intensity are  $600 \mu\text{m}$  and  $7 \times 10^{17} \text{W/cm}^2$ , respectively.

A cluster target was formed by the adiabatic expansion in vacuum of an argon gas puff produced by a pulsed valve with a conical nozzle. Three nozzles with different sizes of input and output holes were tested. The length of the expansion zone was also optimized. Only the arrangement with a 1-mm input diameter, a 8-mm output diameter, and a 20-mm expansion length created the appropriate conditions to obtain a spectrum featuring the x-ray emission from multicharged ions. The laser was focused at the vacuum-gas interface, about 1.5 mm below the nozzle. The gas jet was characterized by laser interferometry. The density profile has a Gaussian shape with a 4-mm width (at  $1/e$ ), and a peak atom density of  $4.6 \times 10^{18} \text{cm}^{-3}$  for a maximum gas backing pressure of 15 bar.

Spatially resolved x-ray spectra of argon in the spectral range 3.35–4.2 Å were obtained by means of two focusing spectrometers with spatial resolution; see Refs. [22–24]. Spherically bent mica crystals with a radius of curvature,  $R = 150$  mm, were used in these spectrometers. The crystal of the first spectrometer was placed 250 mm from the plasma. The middle Bragg angle was  $71.7^\circ$ . Wavelengths near the

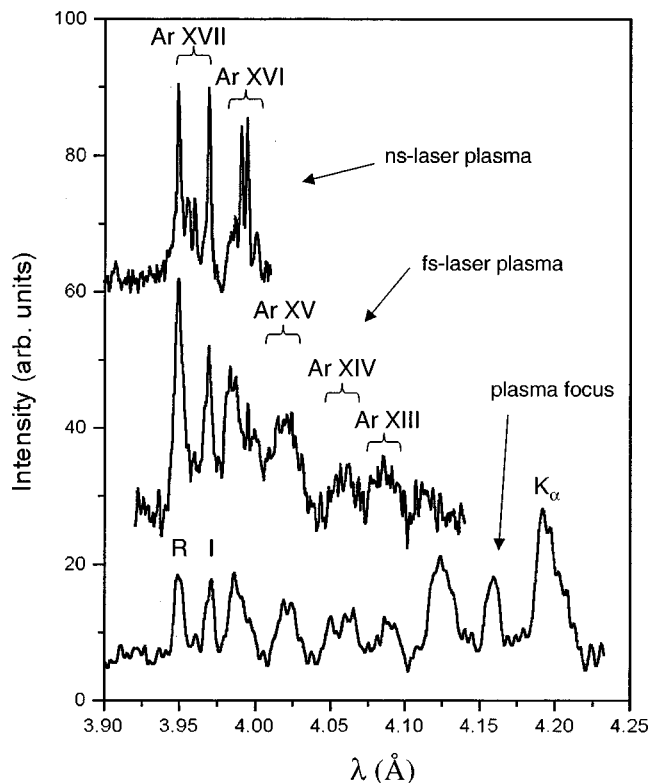


FIG. 1. X-ray emission as a function of wavelength for argon plasma created at different plasma installations: ns-laser-produced plasma [25], plasma focus [26], and fs-laser-produced plasma (present work).

$\text{Ly}_\alpha$  of H-like Ar (3.72–3.82 Å) are in this spectral range, and correspond to the fifth order of the mica crystal reflection. The crystal of the second spectrometer was placed 300 mm from the plasma. The middle Bragg angle was  $56.6^\circ$ . The fifth order of mica crystal reflection allowed recording the spectra near the  $n-n'=3-1$ , and  $4-1$  transitions of He-like Ar XVII. The spectral range between the  $\text{He}_\alpha$  and  $\text{K}_\alpha$  Ar lines was observed in the fourth order of crystal reflection. It should be noted that our attempts to observe the  $\text{Ly}_\alpha$  line of H-like Ar XVIII were unsuccessful.

The theoretical spectral resolution of the fourth and fifth reflection orders of mica crystal approached  $\lambda/\delta\lambda \sim 10000$  for the present of geometry. The x-ray spectral images of Ar have been obtained with a demagnification of about 2.1–2.3 and a spatial resolution around 30–40  $\mu\text{m}$  in the direction of propagation of the laser in the cluster jet, which is consistent with the focusing properties of the spherically bent crystal. The spectra were recorded on Kodak DEF film. The film cassette was protected by two layers of 1- $\mu\text{m}$  polypropylene covered by 0.2  $\mu\text{m}$  of Al, and by a 7- $\mu\text{m}$  Be filter.

An example of the spectra obtained in this experiment is shown in Fig. 1. Spectra observed from earlier experiments are also shown in this figure. These include emission from an argon plasma created by a nanosecond laser [25] and a plasma focus discharge [26]. It is clear from the graphic that the emission spectrum of the femtosecond laser-produced plasma is similar to spectrum radiated from plasma focus. That is, in both cases there are intense satellite structures

caused by transitions in multielectron argon ions (Be-like, B-like, and C-like). However, the nanosecond laser-produced plasma contains mostly emission from only He-like and Li-like argon ions. Moreover, the relative intensities of different Li-like satellites in the femtosecond laser-produced plasma are very similar to those observed in the plasma focus. That is, the intensity of “collisional” satellites designated  $q$ ,  $r$ , and  $a-d$  are greater than the “dielectronic” satellites designated by  $k$  and  $j$ . This differs significantly from the case of the nanosecond plasma, where the intensities of collisional satellites are much less intense than the dielectronic satellites. In review, the main features of the plasma focus are a relatively low plasma temperature and the presence of a powerful electron beam, and these two factors make it possible to describe the experimentally observed spectra [26]. Therefore, it is reasonable to assume that the same features can be attributed to femtosecond laser-produced plasma. It is shown in the present work that this assumption is also adequate for the interaction of the low-contrast femtosecond laser pulse with argon clusters.

### III. RESULTS AND DISCUSSION

#### A. Model of plasma dynamics

Consider the interaction of a high-intensity low-contrast femtosecond laser pulse with argon clusters. In the present experiments, the laser pulse contrast was about  $10^{-5}$ . This means that laser flux density in the prepulse was about  $10^{12-13}$  W/cm<sup>2</sup>. Values of the flux density in this range are enough to destroy clusters and to create plasmas with electron temperatures of a few hundred eV. The spatial distribution of electron density and temperature in the preplasma is formed during the expansion of the clusters heated by the prepulse. This is shown schematically in Fig. 2(a), at the moment just before the arrival of the main pulse. The time of collisional ionization is about 1 ps or less for all argon ions with the number of bound electrons greater than 2, assuming the ionization processes occur in clusters initially having approximately solid density. This means that the preplasma formed must contain He-, Li-, and Be-like argon ions, etc., with an approximately steady ionization state. Note that negligible amounts of H-like Ar XVIII ions are created by the laser prepulse because the ionization rate for  $1s^2$  shell is orders of magnitude smaller than it is for electrons in the  $n = 2$  shell.

The main femtosecond laser pulse then interacts with the nonuniform preplasma. The energy is mainly absorbed in the preplasma by spatial regions where the electron density is greater than or equal to the critical density associated with the laser frequency. As a result, the plasma temperature is sharply increased to a few keV in a small volume within some characteristic dimension  $r_{\text{hot}}$ , while the plasma temperature in the other regions remains low [see Fig. 2(b)]. Thus, during the action of the main pulse, some hot spots are created in the plasma. The distance  $r_{\text{cold}}$  between these hot spots is approximately equal to the distance between clusters in the jet, and the dimension  $r_{\text{hot}}$  has the same order of magnitude as the initial cluster size. This is a very important point because the bulk plasma ionization state is not signifi-

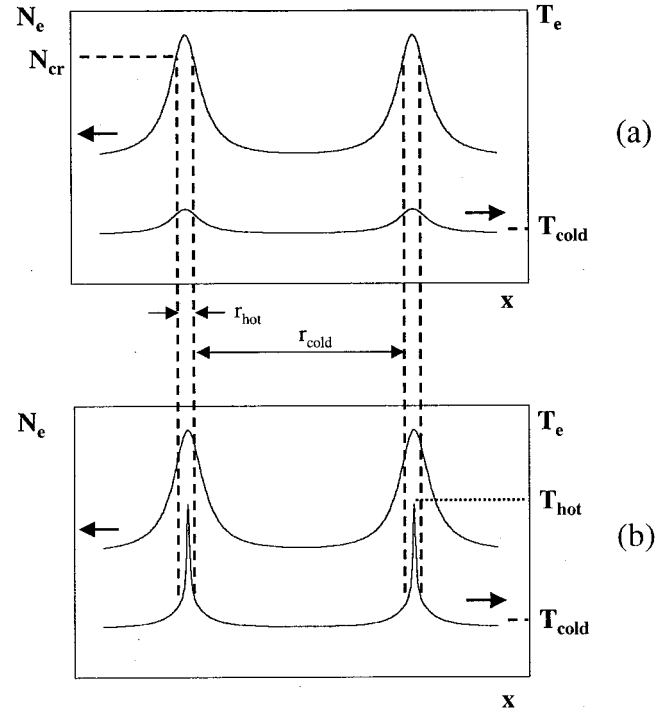


FIG. 2. Plasma creation by a femtosecond laser pulse with a picosecond prepulse. (a) Plasma parameters formed by a prepulse. (b) Additional dense plasma regions heated by the main pulse.

cantly changed during plasma heating because of the short duration of the femtosecond pulse.

After the main pulse ends, hot electrons persist in the plasma. The relative amount of these electrons is about  $(r_{\text{hot}}/r_{\text{cold}})^3 \sim 10^{-8} - 10^{-6}$ . The temperatures of these electrons range from 5 to 10 keV according to previous calculations [27,28]. It is important that the thermalization time scale for these electrons is in excess of tens of picoseconds even in plasmas with critical densities of  $10^{21}$  cm<sup>-3</sup>, and their mean free path is greater than several hundred microns. This means that there will exist both low and high density regions in the plasma for an extended period of time after the end of femtosecond pulse. A low-density plasma characterized by two temperatures will exist where most of the electrons will possess an electron temperature  $T_{\text{cold}}$  (a few hundred eV) and a small fraction of electrons will possess an electron temperature  $T_{\text{hot}}$  (on the order of a several keV). Also, a denser and hotter localized plasma will exist with temperature  $T_e = T_{\text{hot}}$  and with a nonstationary ionization state corresponding to temperature  $T_{\text{cold}}$ . Note that hot electrons will not only be present in the initial hot spot regions, but they will occupy the entire plasma volume because the free path of the hot electrons is greater than total plasma size.

The simplified picture of plasma dynamics described above is rather complicated. It is possible to construct a simpler model more suitable for calculating the emission spectra. This model is based on the above considerations, and takes into account the main features of the interaction of laser pulse with the clusters, but it uses a very simple description of the temporal and spatial distribution of the

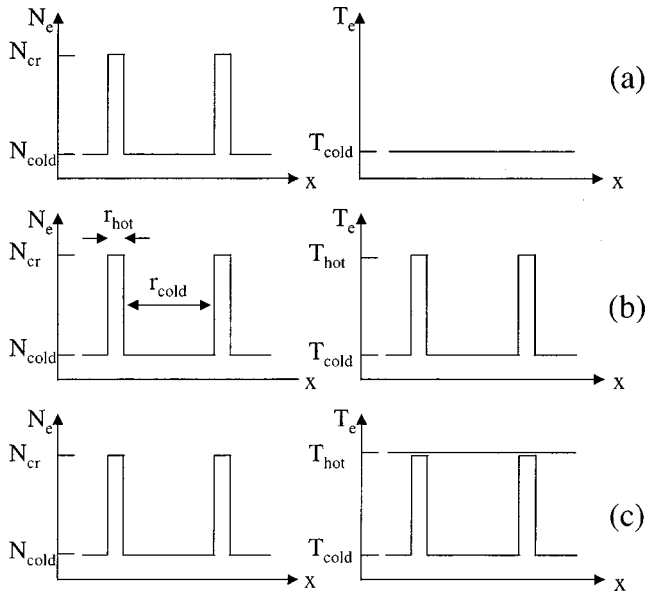


FIG. 3. Schematic diagram of the plasma parameter distribution used for the spectral simulations.

plasma parameters. Here three stages of plasma evolution are considered.

(a) Preplasma stage. The plasma contains dense regions with dimension  $r_{\text{hot}}$  and with electron density  $N_{\text{cr}} = 10^{21} \text{ cm}^{-3}$ . The distance between dense regions is  $r_{\text{cold}}$ , and the plasma electron density outside the dense regions is  $N_{\text{cold}} = 10^{20} \text{ cm}^{-3}$ . The temperature of the plasma is  $T_{\text{cold}}$  for all regions. The plasma ionization state is stationary and corresponds to  $T_{\text{cold}}$ . The duration of this stage is  $t_1 \sim 1 \text{ ps}$ .

(b) Main pulse heating stage. The temperature of the dense regions is equal to  $T_{\text{hot}}$ . The parameters of the cold plasma regions and plasma ionization-state remain the same as in stage (a). The duration of this stage is  $t_{\text{las}} \ll t_1$ .

(c) Decay stage. Hot electrons generated in the dense regions during stage (b) expand into the entire plasma volume. Plasma parameters in the dense regions are the same as in stage (b) ( $N_e = 10^{21} \text{ cm}^{-3}$ ,  $T_e = T_{\text{hot}}$ ). The plasma has a density  $10^{20} \text{ cm}^{-3}$  outside of the dense regions, and a bulk temperature  $T_{\text{cold}}$  with a small amount,  $(r_{\text{hot}}/r_{\text{cold}})^3 = 10^{20} \text{ cm}^{-3}$ , of hot electrons with a temperature  $T_{\text{hot}}$ . The duration of this stage is  $t_2 \sim t_1 \gg t_{\text{las}}$ .

These plasma profiles are presented in Fig. 3. They have been used as a guide for the spectral simulations of plasma emission. Note, that the spectra calculated depend on the plasma densities, temperatures and on the parameters  $\tau = t_1/t_2$  and  $\beta = (r_{\text{hot}}/r_{\text{cold}})^3$ . The exact values of these parameters are unknown. Simple analysis provides only an order of magnitude estimate of  $\tau \sim 1$  and  $\beta \sim 10^{-8} - 10^{-6}$ . Values for both  $\tau$  and  $\beta$  were chosen by comparing the simulated spectra with experiment.

### B. Kinetic calculations

The system of steady-state radiative-collisional rate equations was solved for a uniform plasma with different values of plasma parameters. Multicharged argon ions with a total number of bound electrons  $m = 1, 2, 3,$  and  $4$  were taken into

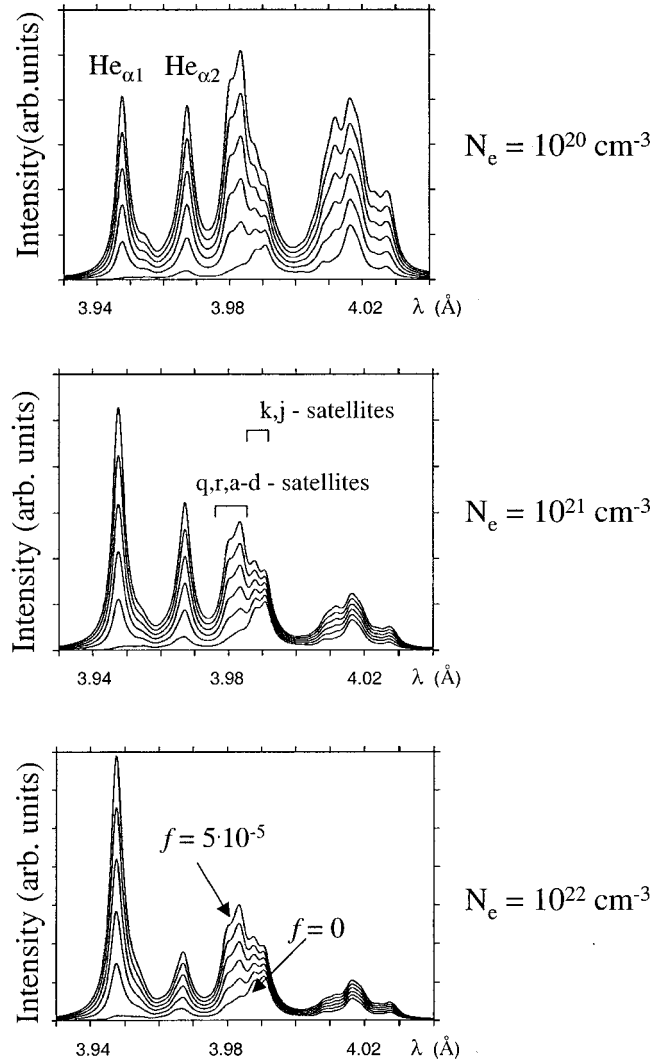


FIG. 4. X-ray emission as a function of wavelength for argon plasma with a bulk electron temperature  $T_e = 190 \text{ eV}$  and different values of electron density  $N_e$  ( $10^{20}$ ,  $10^{21}$ , and  $10^{22}$ ) and hot electron fraction  $f$  ( $0$ ,  $10^{-5}$ ,  $2 \times 10^{-5}$ ,  $3 \times 10^{-5}$ ,  $4 \times 10^{-5}$ , and  $5 \times 10^{-5}$ ) of 5-keV electrons.

account. Atomic configurations with principal quantum numbers  $n < 6$  were considered for H-, He-, Li-, and Be-like ions, including autoionizing states. The calculations included 25 H-like levels, 59 He-like levels, 334 Li-like levels, and 1188 Be-like levels. The rate coefficients for the electron collision processes were calculated using a model electron-energy distribution function [19–20], which includes a provision for hot electrons. The relatively long thermalization time for hot electrons make it possible to consider them as an electron beam with a Gaussian distribution centered around an energy  $E_0$ . Note that the value  $E_0 = 5 \text{ keV}$  was used in the present calculations. The relative amount of hot electrons (designated by  $f$  in Figs. 4 and 5) was varied from 0 (one-temperature plasma) to  $5 \times 10^{-5}$ . The plasma emission spectra were calculated for spectral region  $3.93 - 4.04 \text{ \AA}$ , which was the region observed experimentally. Examples of the results are presented in Figs. 4 and 5.

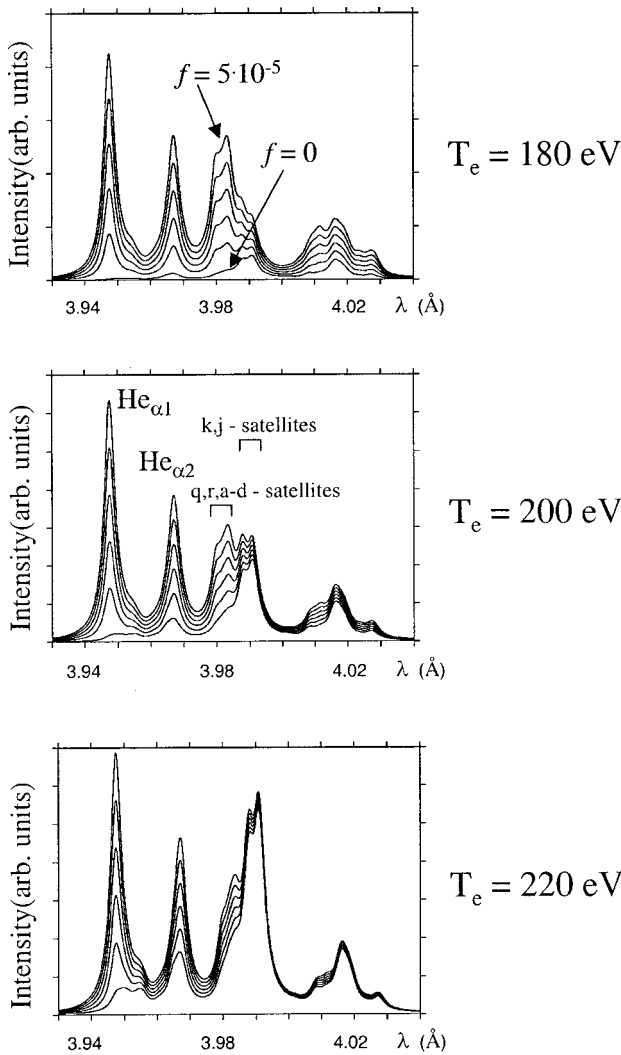


FIG. 5. X-ray emission of argon plasma with an electron density  $N_e = 10^{21} \text{ cm}^{-3}$  and different values of electron temperature  $T_e$  and hot electron fraction  $f$  ( $0, 10^{-5}, 2 \times 10^{-5}, 3 \times 10^{-5}, 4 \times 10^{-5},$  and  $5 \times 10^{-5}$ ) of 5-keV electrons.

Figure 4 shows the dependence of argon emission on plasma electron density. It can be seen from this figure for the one-temperature case ( $f=0$ ), that increasing the plasma density up to  $10^{22} \text{ cm}^{-3}$  does not significantly change the structure of the plasma radiation in the spectral region near the  $\text{He}_\alpha$  line and its satellites.

Figure 5 demonstrates the dependence of spectra on electron temperature. This figure illustrates that the spectrum is more sensitive to temperature than to the plasma density at  $f=0$ . The figure also shows that the influence of hot electrons diminishes as the temperature is increased.

From both Figs. 4 and 5 it can be seen that when hot electrons are absent ( $f=0$ ) the intensities of Li-like satellites  $k$  and  $j$  are much greater than intensity of  $q$ ,  $r$ , and  $a-d$  satellites. The domination of the collisional  $q$ ,  $r$ , and  $a-d$  satellites in the observed spectra are due to enhanced excitation in the presence of hot electrons, at the moderate densities encountered here. This feature can also be observed in superdense plasmas, but with electron densities that exceed

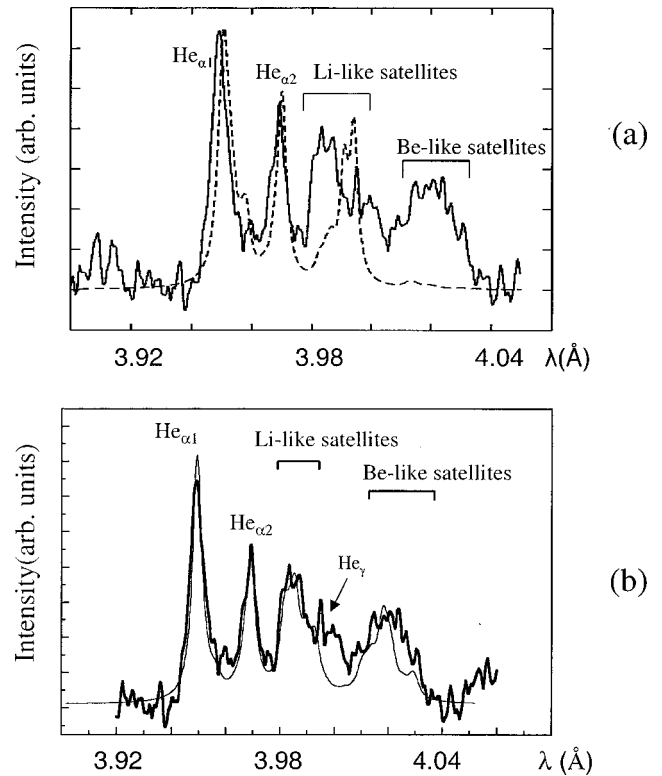


FIG. 6. (a) Comparison of a calculated spectrum (dashed line) for a one-temperature steady-state argon plasma with  $T_e = 550 \text{ eV}$  and  $N_e = 10^{21} \text{ cm}^{-3}$ , with the experimental spectrum (solid line) observed in a femtosecond laser-produced plasma. (b) Comparison of the observed spectrum (thick line) as a function of wavelength in the region  $3.92\text{--}4.06 \text{ \AA}$ , with the result of the simulation (thin line) made for the plasma parameters shown in Fig. 3.

$10^{23} \text{ cm}^{-3}$ . For example, Fig. 6(a) shows a one-temperature steady-state calculation together with the experimental spectrum. The temperature and density were chosen to give the approximate relative intensities of the resonance, intercombination, and Li-like satellites. It is obvious that the one-temperature case cannot explain both the structure of Li-like satellites and the existence of Be-like satellites.

### C. Comparison of the computational results with the observed spectrum

Results of kinetic calculations considered above were used to simulate the plasma emission spectra observed in our experiments. Since the experimental data were obtained without temporal resolution and the plasma was not homogeneous, it was necessary to calculate emission spectra for all plasma spatial regions for all moments of time, and to sum the results to produce total plasma radiation. The spatial and temporal properties of the plasma were modeled using the simple dependencies shown in Fig. 3. The values  $T_{\text{cold}} = 190 \text{ eV}$  and  $T_{\text{hot}} = 5 \text{ keV}$  were used.

Figure 6(b) shows that the experimental spectra are represented very well by the simulation if the value of  $\tau = t_1/t_2$  is chosen to be 1 and the value of  $\beta = (r_{\text{hot}}/r_{\text{cold}})^3$  is chosen to be  $4 \times 10^{-7}$ . The discrepancies in the two curves in Fig. 6(b) can be attributed in part to the presence of the

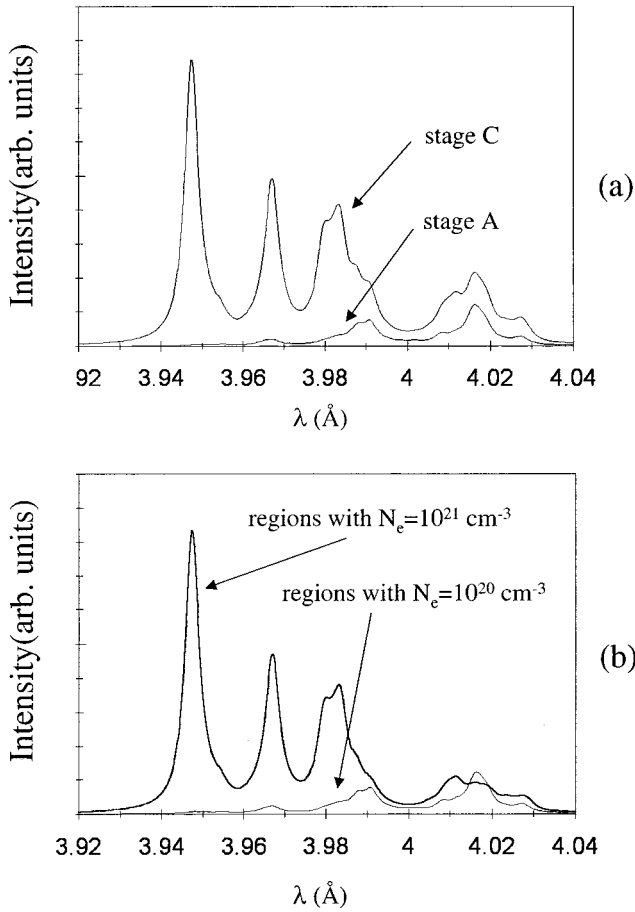


FIG. 7. (a) Argon plasma emissions caused by different stages of plasma evolution. (b) Emission of different spatial plasma regions during stage C (after heating by the main fs-laser pulse).

$\text{He}_\gamma$  line of Ar XVIII ( $\lambda=3.1996 \text{ \AA}$ ) in the experimental spectrum. This line is observed in the fifth order of crystal reflection and therefore comes from another spectral region, and hence is not included in the theoretical result.

The theoretical spectrum presented in Fig. 6(b) is the sum of spectra emitted by different plasma regions at different moments of time. It is very interesting to understand which stage of plasma evolution gives the main contribution to the total plasma emission. In Fig. 7(a), the simulation results are presented separately for both stages (a) and (c). Note that duration of stage (b) is so short that its contribution is negligible. It is apparent that the main part of plasma radiation is emitted during stage (c). The preplasma stage (a) is essential only for producing the Be-like satellites and Li-like ‘dielectronic’ satellites  $k, j$ .

Figure 7(b) illustrates the contributions of the various spatial regions that are responsible for the emission of the brightest stage (c). This figure shows that most of the He and Li-like emissions are caused by the most dense plasma regions, and that the low-density plasma is responsible for the Be-like lines and, again, for the  $k$  and  $j$  Li-like transitions.

The model has also to calculate plasma emission in the spectral range 3.35–3.45  $\text{\AA}$ , where the  $\text{He}_\beta$  line of Ar XVII is located. A comparison between the model and experiment is

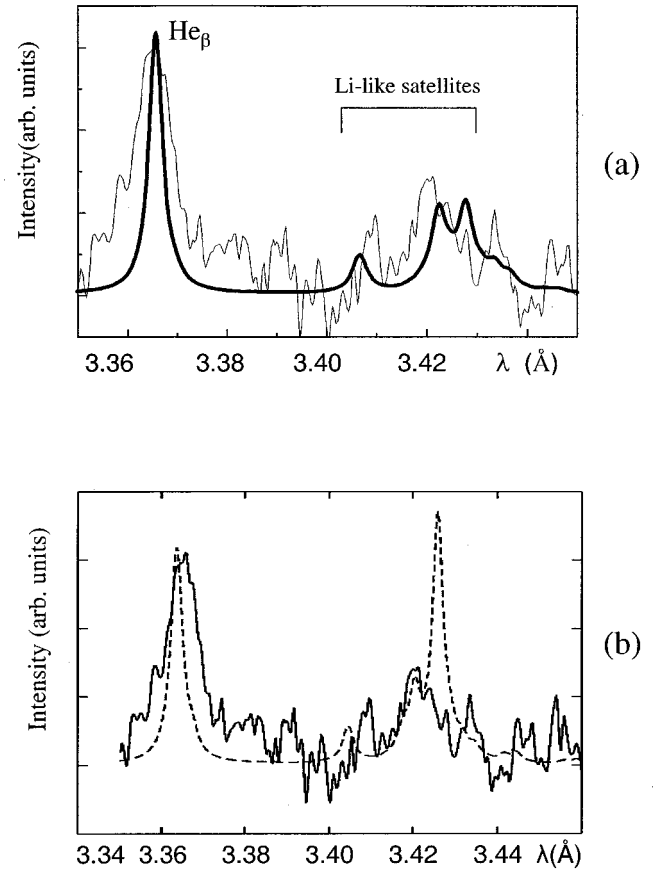


FIG. 8. (a) Comparison of the spectrum (thin line) observed in the region of the  $\text{He}_\beta$  line (3.35–3.45  $\text{\AA}$ ), with the result of the simulation (thick line) made for plasma parameters shown in Fig. 3. (b) Comparison of  $\text{He}_\beta$  emission calculated (dashed line) for a one-temperature ( $f=0$ ) steady-state argon plasma with  $T_e=550 \text{ eV}$  and  $N_e=10^{21} \text{ cm}^{-3}$  with experiment (gray line).

shown in Fig. 8(a). Note that the model, with the same plasma parameters that were used for calculation in Fig. 6(b), gives reasonable agreement with the experimental spectrum. Figure 8(b) shows a comparison of the one-temperature steady-state model using the plasma parameters of Fig. 6(a) with experiment. Note that the model cannot adequately describe the experimental data for both the  $\text{He}_\alpha$  [see Fig. 6(a)] and the  $\text{He}_\beta$  [see Fig. 8(b)] emission.

The model calculations predict that a negligible amount of H-like Ar XVIII ions were produced in the plasma. This is in agreement with the fact that  $\text{Ly}\alpha$  Ar XVIII line was not observed.

The good agreement between theoretical and experimental data provides proof of the presence of hot electrons in cluster plasmas created by a high-intensity femtosecond laser pulse. In general, it is possible to measure the average hot-electron energy from comparison experimental spectra with model simulations. However, the dependence of emission spectra on the hot-electron energy is approximately defined by the parameter  $(r_{\text{hot}}/r_{\text{cold}})^3 \exp(-E_{\text{exc}}/T_{\text{hot}})/T_{\text{hot}}^{0.5}$  and therefore we must know the ratio  $(r_{\text{hot}}/r_{\text{cold}})^3$  which represents the relative amount of hot electrons for the determina-

tion of  $T_{\text{hot}}$ . Unfortunately, we cannot obtain this ratio independently from our measurements.

#### IV. CONCLUSIONS

In the present paper, we show that the interaction of a high-intensity femtosecond laser pulse having a picosecond prepulse with argon clusters can be successfully used to obtain a bright plasma source of x-ray radiation. Initially, it would appear that our result contradicts the conclusion made in Ref. [1]. However, there is a big difference between the experiments carried out in Ref. [1] and those presented here. In Ref. [1] the laser prepulse duration was several nanoseconds. This is enough time to destroy the clusters entirely, and at the arrival of the main pulse there were no plasma regions near the critical density. Under these conditions, only a small amount of the main laser pulse is absorbed by plasma, and hence no x-ray radiation was detected. In the present experiments, however, the prepulse duration was only several picoseconds, which is not long enough to produce a uniform

low-density nonabsorbing plasma. Thus only short prepulses can be used to produce effective “plasma targets.” The critical value for the prepulse duration  $\tau_{\text{crit}}$  depends, of course, on the initial cluster size and on the velocity of cluster expansion. Typically, the value of  $\tau_{\text{crit}}$  is about 1 ps.

The cluster target makes it possible to produce plasmas having a moderate ionization state, defined by the laser prepulse flux density of a picosecond duration, and containing a hot-electron fraction whose energy is determined by the flux density of the main femtosecond pulse. It may be possible to obtain plasmas with pre-specified conditions by varying the prepulse–pulse intensity ratio. This plasma source can be used to study the spectral transitions driven by high-energy electrons in underionized plasmas, especially for studies of emission by multicharged ions with inner-shell vacancies.

#### ACKNOWLEDGMENT

This work was performed, in part, under the auspices of the U.S. Department of Energy.

- 
- [1] T. Ditmire, T. Donnelly, A. M. Rubenchik, R. W. Falcone, and M. D. Perry, *Phys. Rev. A* **53**, 3379 (1996).
- [2] P. Gibbon and E. Forster, *Plasma Phys. Controlled Fusion* **38**, 769 (1996).
- [3] T. Ditmire, J. Zweiback, V. P. Yanovsky, T. E. Cowan, G. Hays, and K. B. Wharton, *Nature (London)* **398**, 489 (1999).
- [4] A. McPherson, B. D. Thompson, A. B. Borisov, K. Boyer, and C. K. Rhodes, *Nature (London)* **370**, 631 (1994).
- [5] T. Ditmire, R. A. Smith, J. W. G. Tisch, and M. H. R. Hutchinson, *Phys. Rev. Lett.* **78**, 3121 (1997).
- [6] Y. L. Shao, T. Ditmire, J. W. G. Tisch, E. Springate, J. P. Marangos, and M. H. R. Hutchinson, *Phys. Rev. Lett.* **77**, 3343 (1996).
- [7] T. Ditmire, J. W. G. Tisch, E. Springate, M. B. Mason, N. Hay, R. A. Smith, J. P. Marangos, and M. H. R. Hutchinson, *Nature (London)* **386**, 54 (1997).
- [8] T. Ditmire, J. W. G. Tisch, E. Springate, M. B. Mason, N. Hay, J. P. Marangos, and M. H. R. Hutchinson, *Phys. Rev. Lett.* **78**, 2732 (1997).
- [9] E. M. Snyder, S. A. Buzza, and A. W. Castleman, Jr., *Phys. Rev. Lett.* **77**, 3347 (1996).
- [10] S. Dobosz, M. Schmidt, M. Pedrix, P. Meynadier, O. Gobert, D. Normand, A. Ya. Faenov, A. I. Magunov, T. A. Pikuz, I. Yu. Skobelev, and N. E. Andreev, *Pis'ma Zh. Eksp. Teor. Fiz.* **68**, 454 (1998) [*JETP Lett.* **68**, 485 (1998)].
- [11] S. Dobosz, M. Schmidt, M. Perdrix, P. Meynadier, O. Gobert, D. Normand, K. Ellert, T. Blenski, A. Ya. Faenov, A. I. Magunov, T. A. Pikuz, I. Yu. Skobelev, and N. E. Andreev, [*JETP* **88**, 1122 (1999)].
- [12] J. Zweiback, R. A. Smith, T. E. Cowan, G. Hays, K. B. Wharton, V. P. Yanovsky, and T. Ditmire, *Phys. Rev. Lett.* **84**, 2634 (2000).
- [13] A. Ya. Faenov, J. Abdallah, Jr., R. E. H. Clark, J. Cohen, R. P. Johnson, G. A. Kyrala, A. I. Magunov, T. A. Pikuz, I. Yu. Skobelev, and M. D. Wilke, *Proc. SPIE* **3157**, 10 (1997).
- [14] A. M. Urnov, J. Dubau, A. Ya. Faenov, T. A. Pikuz, I. Yu. Skobelev, J. Abdallah, Jr., R. E. H. Clark, J. Cohen, R. P. Johnson, G. A. Kyrala, M. D. Wilke, and A. L. Osterheld, *Pis'ma Zh. Eksp. Teor. Fiz.* **67**, 467 (1998) [*JETP Lett.* **67**, 489 (1998)].
- [15] A. Ya. Faenov, A. I. Magunov, T. A. Pikuz, I. Yu. Skobelev, S. A. Pikuz, A. M. Urnov, J. Abdallah, R. E. H. Clark, J. Cohen, R. P. Johnson, G. A. Kyrala, M. D. Wilke, A. Maksimchuk, D. Umstadter, N. Nantel, R. Doron, E. Behar, P. Mandelbaum, J. J. Schwob, J. Dubau, F. B. Rosmej, and A. Osterheld, *Phys. Scr.* **T80**, 536 (1999).
- [16] A. Maksimchuk, M. Nantel, G. Ma, S. Gu, C. Y. Cote, D. Umstadter, S. A. Pikuz, I. Yu. Skobelev, and A. Ya. Faenov, *J. Quant. Spectrosc. Radiat. Transf.* **65**, 367 (2000).
- [17] F. B. Rosmej, U. N. Funk, M. Geißel, D. H. H. Hoffmann, A. Tauschwitz, A. Ya. Faenov, T. A. Pikuz, T. Yu. Skobelev, I. Flora, S. Bollanti, P. Di Lazzaro, T. Letardi, A. Grilli, L. Palladino, A. Reale, G. Tomassetti, A. Scafati, L. Reale, T. Auguste, P. D'Oliveira, S. Hulin, P. Monot, A. Maksimchuk, S. A. Pikuz, D. Umstadter, M. Nantel, R. Bock, M. Dornik, M. Stetter, S. Stöwe, V. Yakushev, M. Kulisch, and N. Shilkin, *J. Quant. Spectrosc. Radiat. Transf.* **65**, 477 (2000).
- [18] A. G. Zhidkov, A. Sasaki, T. Tajima, T. Auguste, P. D'Oliveira, S. Hulin, P. Monot, A. Ya. Faenov, T. A. Pikuz, and I. Yu. Skobelev, *Phys. Rev. E* **60**, 3273 (1999).
- [19] J. Abdallah, Jr., R. E. H. Clark, A. Ya. Faenov, L. Karpinski, S. A. Pikuz, V. M. Romanova, M. Sadowski, M. Scholz, and A. Szydlowski, *J. Quant. Spectrosc. Radiat. Transf.* **62**, 85 (1999).
- [20] J. Abdallah, Jr., A. Ya. Faenov, T. A. Pikuz, M. D. Wilke, G. A. Kyrala, and R. E. H. Clark, *J. Quant. Spectrosc. Radiat. Transf.* **62**, 1 (1999).
- [21] S. A. Pikuz, T. A. Shelkovenko, V. M. Romanova, J. Abdal-

- lah, Jr., G. Csanak, R. E. H. Clark, A. Ya. Faenov, I. Yu. Skobelev, and D. A. Hammer, *JETP* **85**, 484 (1997).
- [22] I. Yu. Skobelev, A. Ya. Faenov, B. A. Bryunetkin, V. M. Dyakin, T. A. Pikuz, S. A. Pikuz, T. A. Shelkovenko, and V. M. Romanova, *Zh. Eksp. Teor. Fiz.* **108**, 1263 (1995) [*JETP* **81**, 692 (1995)].
- [23] T. A. Pikuz, A. Ya. Faenov, S. A. Pikuz, V. M. Romanova, and T. A. Shelkovenko, *J. X-Ray Sci. Technol.* **5**, 323 (1995).
- [24] B. K. F. Young, A. L. Osterheld, D. F. Price, R. Shepherd, R. E. Stewart, A. Ya. Faenov, A. I. Magunov, T. A. Pikuz, I. Yu. Skobelev, F. Flora, S. Bollanti, P. Di Lazzaro, T. Letardi, A. Grilli, L. Palladino, A. Reale, A. Scafati, and L. Reale, *Rev. Sci. Instrum.* **69**, 4049 (1998).
- [25] V. M. Dyakin, I. Yu. Skobelev, A. Ya. Faenov, A. Bartnik, H. Fiedorowicz, M. Szczurek, A. Osterheld, and J. Nilsen, *Quantum Electron.* **27**, 691 (1997).
- [26] E. Biemont, P. Quinet, A. Ya. Faenov, I. Yu. Skobelev, J. Nilsen, V. M. Romanova, M. Scholz, L. Karpinski, and A. Szydlowski, *Phys. Scr.* (to be published).
- [27] T. Ditmire, P. K. Patel, R. A. Smith, J. S. Wark, S. J. Rose, D. Milathianaki, R. S. Marjoribanks, and M. H. R. Hutchinson, *J. Phys. B* **31**, 2825 (1998).
- [28] R. A. Smith, J. W. G. Tisch, T. Ditmire, E. Springate, N. Hay, M. B. Mason, E. T. Gumbrell, A. J. Comley, L. C. Mountford, J. P. Marangos, and M. H. R. Hutchinson, *Phys. Scr.* **T80**, 35 (1999).